JOURNAL OF MATERIALS SCIENCE 32 (1997) 4101–4107

Microsegregation and solidification cracking of an HR-160 weld overlay

J. N. DUPONT
Lehigh University, Bethlehem, PA, USA

The solidification behaviour (microsegregation, secondary phase formation, solidification temperature range) of a Haynes HR-160 weld overlay deposited on 2.25 Cr–IMo steel by gas metal arc welding has been examined. Results of differential thermal analysis and various microscopy techniques conducted on an all-weld-metal sample indicate the overlay terminates solidification at $\approx$1290 °C by the formation of a (Ti–S)-rich second phase distributed semi-continuously along grain boundaries. The semi-continuous morphology of the second phase, combined with an increase in the solidification temperature range induced by the second phase, promoted solidification cracking in the overlay deposit. Electron probe microanalysis (EPMA) was used to reveal patterns of elemental segregation within the weld overlay. The EPMA data was used with basic solidification theory to estimate values for equilibrium distribution coefficients of major alloying elements and the values are found to be similar to results previously reported for Incoloy 909.

1. Introduction

Alloy HR-160 is a Ni–Co–Cr alloy with relatively high silicon additions ($\approx$ 2.7 wt %) designed for good corrosion resistance in sulfidizing atmospheres. Corrosion studies conducted by Lai [1] have shown the alloy can form a protective oxide scale even in aggressive sulfidizing environments at 870 °C where $P_{O_2} = 3.039 \times 10^{-14}$ Pa and $P_{S_2} = 9.117 \times 10^{-2}$ Pa. Norton [2] generated gravimetric data at 700 °C with $P_{O_2} = 1.013 \times 10^{-18}$ Pa and $P_{S_2} = 1.073 \times 10^{-4}$ Pa which demonstrated that Alloy HR-160 exhibits corrosion rates significantly lower than other austenitic alloys such as HR-120, Alloy 800, Alloy 556 and Type 347 stainless steel. The ability to form a protective oxide scale and exhibit good corrosion resistance in such environments with low oxygen partial pressures makes this alloy an attractive candidate for several industrial applications. Examples include coal gasification and fossil-fired boilers operating with low NOx burners where enhanced sulfidation corrosion can occur [3]. In these operating environments, application of a corrosion resistant coating by weld overlay processes provides a method of protecting existing, less corrosion resistant components subjected to sulfidation. In such applications, candidate weld overlay alloys must posses good sulfidation resistance combined with good resistance to solidification cracking. The presence of solidification cracks in the overlay coating provides potential paths for sulfidizing gases to reach the substrate, significantly compromising the effectiveness of the coating.

Solidification cracking susceptibility is known [4] to be controlled mainly by the solidification temperature range and amount and distribution of secondary phases that form at the terminal stages of solidification. Each of these factors (solidification temperature range and amount of second phase) are controlled by the microsegregation behaviour of the given alloy during solidification. The degree of microsegregation in the final weld overlay is also of considerable importance with regards to possible effects on corrosion performance. Since corrosion resistance is highly composition-dependent, the extent of local variations in composition within the dendritic substructure due to microsegregation should be considered. However, no information exists on the microsegregation behaviour of this alloy/substrate combination under solidification conditions typical of welding. Thus, in this work, the solidification behaviour of an HR-160 weld overlay deposited on 2.25 Cr–1Mo steel is investigated.

2. Experimental procedure

The chemical composition of the HR-160 consumable electrode and 2.25 Cr–1Mo substrate are given in Table I. The overlay was prepared by the gas metal arc welding process using a 1.14 mm diameter electrode and 6.4 mm thick 2.25 Cr–1Mo steel substrate using the following parameters: 30 V, 230 A (175 mm s^{-1} electrode velocity), 16 mm s^{-1} travel speed, and argon shielding gas. Voltage was measured between the torch contact tube and substrate and thus represents the combined voltage drops between the arc and electrode. Multiple passes were applied with a 50% overlap between passes while maintaining a 100–150 °C interpass temperature.

Light optical microscopy (LOM), scanning electron microscopy (SEM), and electron probe microanalysis (EPMA) were conducted on a sample removed from

0022–2461

TABLE I Chemical composition of HR-160 electrode and 2.25Cr–1Mo steel

Element	HR-160 filler alloy	2.25Cr–1Mo substrate
Iron	1.40	94.85
Nickel	36.84	< 0.01
Chromium	27.61	2.06
Cobalt	30.55	< 0.01
Silicon	2.68	0.27
Molybdenum	0.14	0.90
Manganese	0.43	0.43
Titanium	0.46	< 0.01
Phosphorus	< 0.001	0.024
Sulfur	0.001	0.014
Carbon	0.045	0.132

All values in weight %.

the overlay. The sample was polished to a 0.04 μm finish using colloidal silica and etched electrolytically in a 10% chromic acid/90% water solution at ≈ 3 V. Scanning electron microscopy was conducted at an accelerating voltage of 20 kV. After observation by LOM and SEM, small areas of parallel cellular dendrites were bracketed for EPMA by microhardness indentations. The sample was then re-polished to a 0.04 μm finish and carbon coated. Electron probe microanalysis was conducted at an accelerating voltage of 15 kV and beam current of ≈20 nA. The K_α lines were used for all elements except Mo, in which the L_α line was used. Raw data were reduced to weight percentages using a ZAF algorithm.

A sample of all weld metal was obtained by machining away the substrate. The sample was used for bulk chemical analysis and differential thermal analysis (DTA). The DTA was conducted on Netzsch STA 409 thermal analyser using argon cover gas and an alumina crucible. The sample size was ≈1.2 g and pure Ni was used as the reference material. The sample was heated to 1440 °C at a rate of 5 °C min^{-1} at which point it was completely molten. The alloy was then cooled at 20 °C min^{-1} through the solidification temperature range to simulate non-equilibrium solidification as closely as possible within the equipment cooling rate capacity. The weight of the sample was simultaneously monitored by a thermogravimetric balance to ensure no weight change occurred during the test. The DTA system was calibrated by determining the melting temperature of pure Ni and found to be within 2 °C of the literature value. Reaction temperatures were taken as deviations from the local baseline. LOM, SEM, and energy dispersive spectrometry (EDS) were conducted on the DTA specimen by the procedure described above.

3. Results

Fig. 1 shows LOM photomicrographs of typical solidification cracks observed in the overlay. Cracking was found to be rather extensive, with many solidification cracks traversing the entire overlay. The cracks coincided with a semi-continuous second phase located at the grain boundaries (Fig. 1b). Isolated second phase particles also exist in the interdendritic regions. This pattern is typical of hot cracks which form at the terminal stages of solidification [4]. In terms of the second phase, the DTA specimen showed similar behaviour (Figs 2 and 3), where the second phase is observed in a semi-continuous morphology along the grain boundaries. The backscattered electron image shown in Fig. 3b indicates this phase has a low atomic number relative to the matrix. This is confirmed by Fig. 4, which presents a typical energy dispersive spectrum from the grain boundary phase showing it is rich in titanium and sulfur.

Fig. 5 shows an EPMA trace conducted across several cellular dendrites in the overlay. The location of the trace is presented in Fig. 6 and typical dendrite core (DC) and interdendritic (ID) locations are denoted in the plot of Fig. 5b. The dendrite cores are depleted in Si, Mo, Ti, Ni, and Cr and enriched in Co and Fe. EPMA results from a local trace obtained at the fusion line area and a broader trace from the entire weld overlay are presented in Figs 7 and 8, respectively. Near the fusion line, a narrow transition region (≈30 μm) exists where the composition is intermediate between the substrate and overlay compositions. After this region, the overlay exhibits smaller random variations in composition which are associated with the dendritic microsegregation previously shown in Fig. 5. Examination of the major elements in Fig. 8a which show only a slight tendency for dendritic segregation (most notably Co and Cr), indicate that no *macro*segregation exists within the overlay due to incomplete mixing between the consumable electrode and substrate.

Table II lists the results of chemical analysis conducted on the all weld metal deposit. The average values of all the EPMA data collected after the transition region (after position 50 μm in Figs 7 and 8) are shown for comparison. The results from bulk chemical analysis lie within the variation of the EPMA data, which provides additional support that macrosegregation within the weld is insignificant and, thus, the overlay can be considered homogeneous on a bulk scale. This result will be utilized later to experimentally determine equilibrium distribution coefficients for major alloying elements in the weld overlay.

Fig. 9 shows the DTA solidification trace. A large exothermic peak is initiated at 1406 °C (Fig. 9a). Fig. 9b shows an expanded view in the region of 1260 and 1310 °C where a second smaller peak is observed at 1292 °C. These results are consistent with the observed solidification microstructure, which contains primary γ dendrites with a small amount of (Ti, S)-rich second phase. The initiation of the exothermic peak at 1406 °C can be linked to formation of the primary γ dendrites while the smaller peak at 1292 °C is associated with the small amount of grain boundary and interdendritic (Ti, S)-rich second phase.

4. Discussion

4.1. Solidification cracking

The formation of solidification cracks in the weld overlay can be understood in terms of the DTA results, solidification microstructure, and basic hot

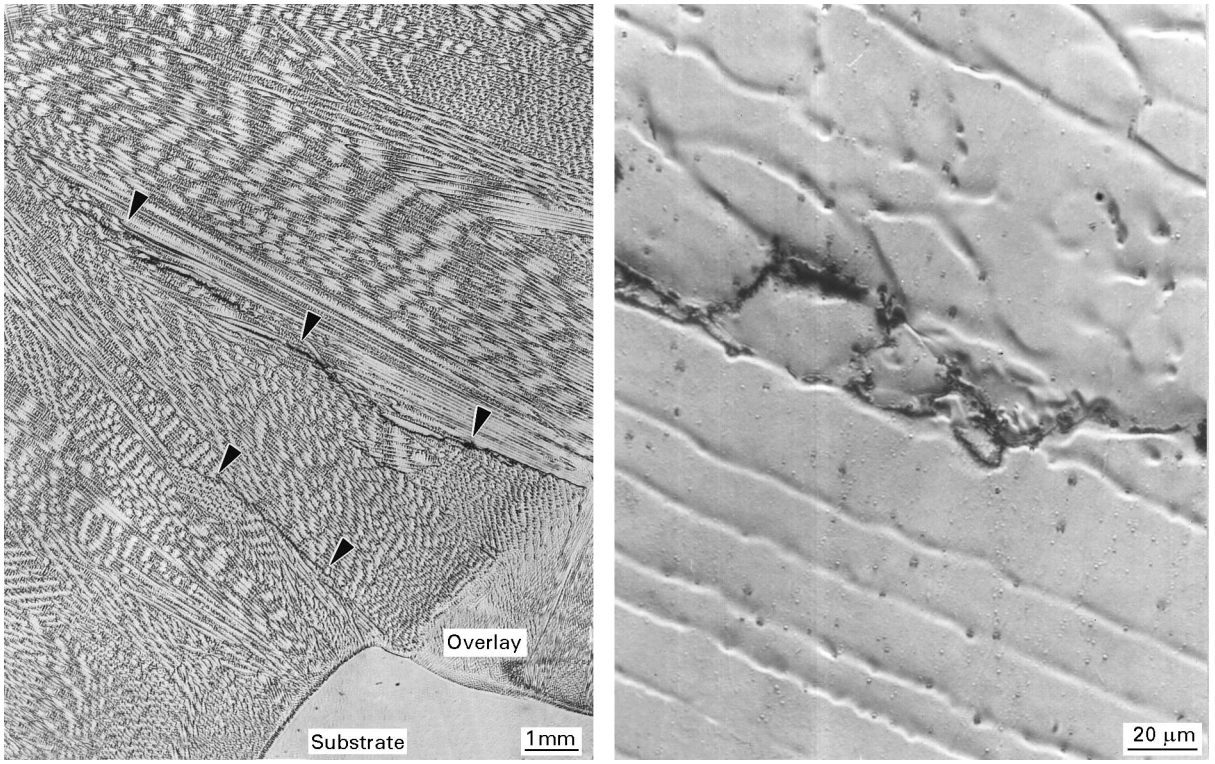

Figure 1 LOM photomicrographs of typical solidification cracks observed in the overlay.

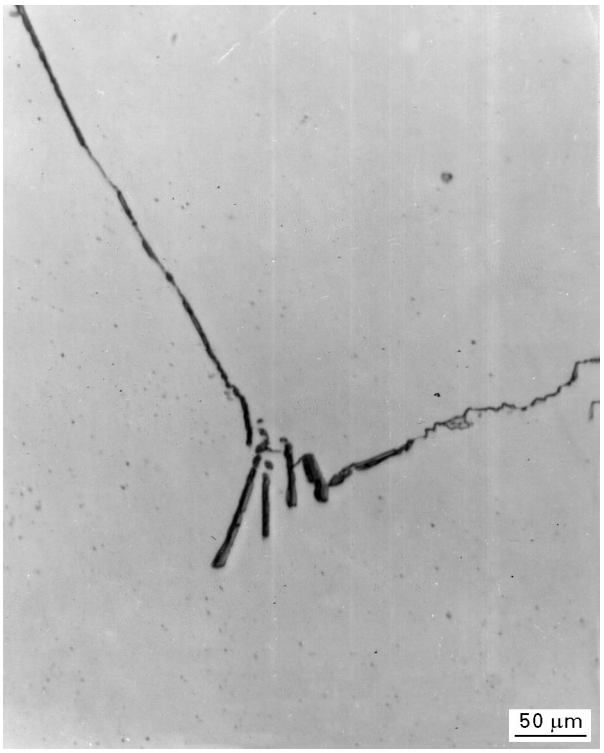

Figure 2 LOM photomicrograph of second phase observed along grain boundaries of DTA sample.

cracking concepts. For a given level of residual strain in the solidifying weld, cracking susceptibility is controlled mainly by the solidification temperature range, the amount of second phase formed at grain boundaries and interdendritic regions at the terminal stages of solidification, and the distribution of that phase [4]. Cracking tendency increases with increasing solidification temperature range and the formation of terminal secondary constituents at levels up to ≈ 7 vol % [5]. When an interdendritic liquid forms in quantities greater than ≈ 7 vol %, back-filling of hot cracks can occur and cracking susceptibility can often decrease [5, 6]. However, the amount of second phase which forms cannot be used as an indicator of cracking susceptibility alone without considering the phase distribution. The primary detrimental effect of the second phase (which exists as a boundary liquid just above the terminal solidus temperature) is to interfere with the formation of solid/solid boundaries which support the residual strain during solidification. Thus, terminal liquids which easily wet the grain boundaries are most harmful to cracking resistance since they are effective in inhibiting formation of solid/solid boundaries [4].

The second phase observed in the solidification microstructure was found to be rich in sulfur and nearly continuous along the grain boundaries. The adverse effect of sulfur on the hot cracking resistance of fully austenitic weld metals has been well documented [7, 8]. This strong effect is associated with two factors: a very low equilibrium distribution coefficient [9], k, and a low liquid/solid interfacial energy [4]. A very low distribution coefficient indicates the element segregates strongly to the liquid phase during solidification. An indication of k for sulfur in fully austenitic welds can be estimated from the Ni–S binary phase diagram, where k_S has been approximated to be of the order of 0.0003 [9]. This value is about three orders of magnitude lower than most other solutes in both Ni binary alloys [9] and multicomponent Ni-base alloys [10, 11]. Thus, even when present in trace quantities, a highly enriched

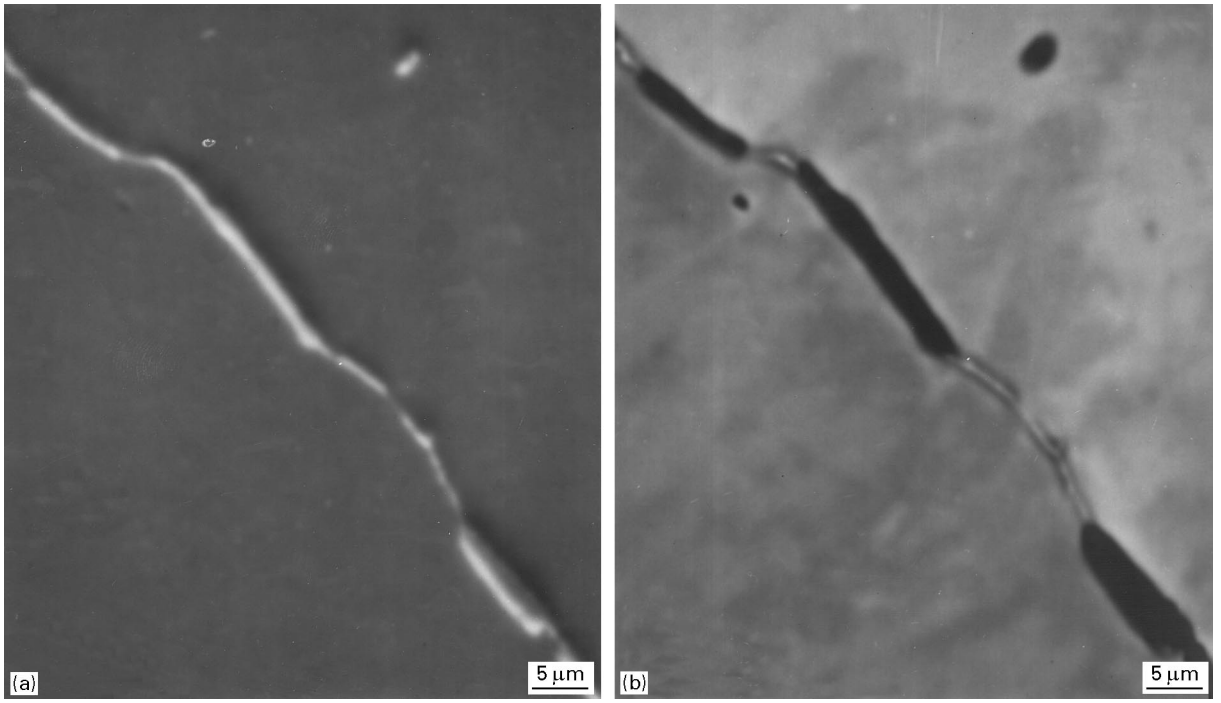

Figure 3 SEM photomicrographs of second phase observed along grain boundaries of DTA sample. (a) Secondary electron image and (b) backscattered electron image.

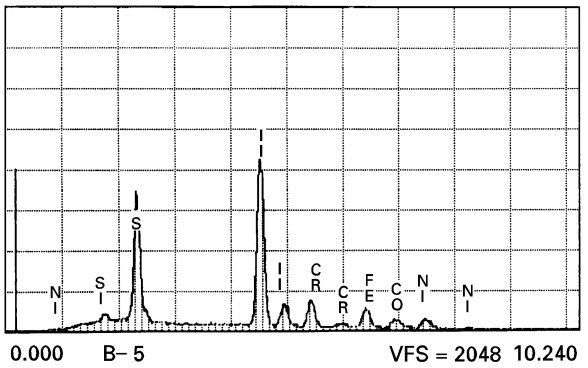

Figure 4 Typical energy dispersive spectrum from the grain boundary phase shown in Fig. 3.

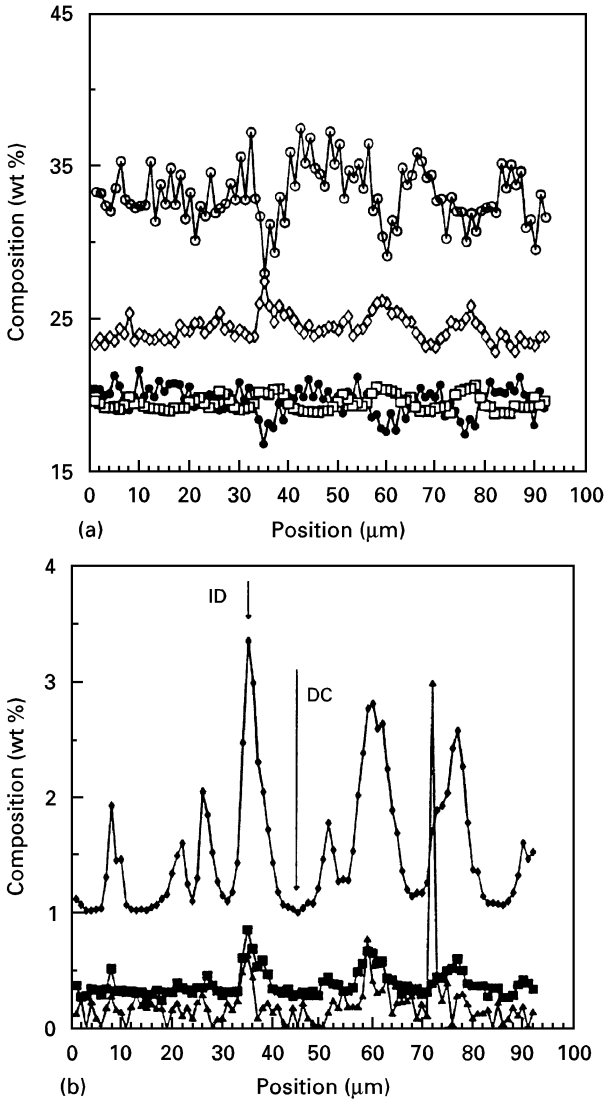

Figure 5 EPMA trace conducted across several cellular dendrites in the overlay. (a) Fe(○), Ni(◇), Co(●), and Cr(□); (b) Si(◆), Mo(■), and Ti(▲).

sulfur region can form in the last regions to solidify since k is so low. Once a S-rich liquid forms at the terminal stages of solidification, the low solid/liquid interfacial energy causes the liquid to be distributed as a nearly continuous grain boundary phase in a morphology which is most harmful. Lastly, the low k value also translates into a wide solidification temperature range since the effective solidus temperature is reduced. This effect is reflected in the DTA trace, where terminal solidification of the (Ti, S)-rich phase occurs at 1292 °C and promotes an extension of the solidification temperature range.

These detrimental effects of sulfur should be considered with respect to the final weld overlay composition as affected by the substrate composition. The sulfur content of Ni-based alloys is typically held to low levels to avoid hot cracking problems, which is reflected in the low sulfur level of the HR-160 filler alloy (Table I). However, Cr–Mo steels are not held to such stringent practices and the sulfur levels are

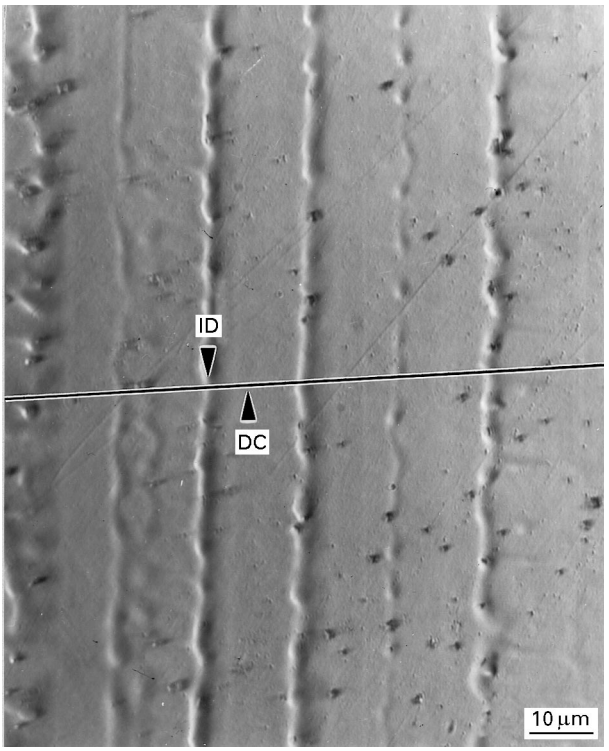

Figure 6 LOM photomicrograph showing location of EPMA trace presented in Fig. 5.

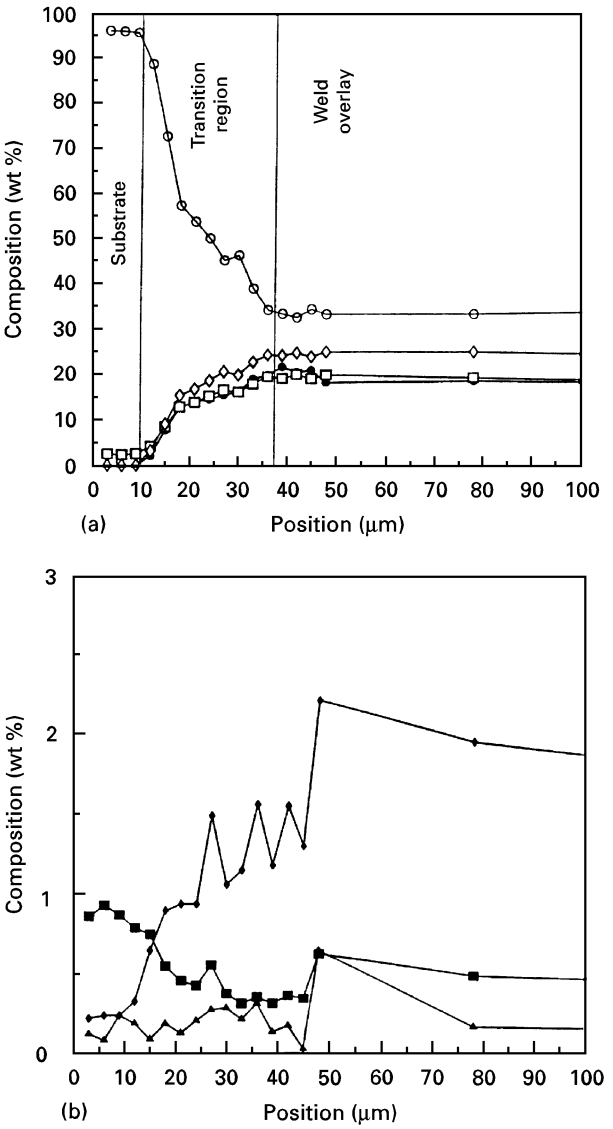

Figure 7 EPMA results from a local trace obtained at the fusion line area. (a) Fe(○), Ni(◇), Co(●), and Cr(□); (b) Si(◆), Mo(■), and Ti(▲).

higher. During welding, substantial amounts of sulfur can be transferred from the substrate to overlay (Table II) and aggravate cracking problems. A similar effect should be considered for phosphorus, which has been shown to significantly increase hot cracking tendency, particularly when combined with sulfur [12]. From this work, the hot-cracking susceptibility of the HR-160 weld overlay appears to be quite sensitive to elevated S (and possibly P) levels. Thus, minimizing dilution in weld overlay applications may aid to reduce cracking susceptibility.

4.2. Microsegregation

The high sulfidation resistance of this alloy is achieved by a careful balance in alloying elements [1]. The Si concentration is particularly important since Si promotes the formation of a protective oxide surface scale. However, when utilized in weld overlay form, the final composition will differ from the HR-160 bulk composition by two factors: dilution from the substrate and microsegregation. Dilution alters the overall weld composition by increasing Fe (from the substrate) at the expense of other elements in the filler alloy (compare the bulk HR-160 composition in Table I and overlay composition in Table II). Dilution is governed by the processing parameters and thermal efficiency of the welding process and a method for estimating dilution from knowledge of these factors has recently been proposed [13]. On the other hand, microsegregation during solidification is governed mainly by the distribution coefficient (k) of the particular element in the overlay and produces localized variations in composition within the dendritic substructure. The extent of segregation for each element can be estimated if the equilibrium distribution coefficient is known. Values of k for the major alloying elements can be estimated from the EPMA data and basic solidification theory.

Microsegregation during solidification can be described with the aid of the Scheil equation [14]

$$C_s = kC_o(1 - f_s)^{k-1} \quad (1)$$

where k is the equilibrium distribution coefficient, defined as the ratio of solid to liquid composition at any temperature, C_s is the solid composition at any fraction solidified, f_s, and C_o is the nominal composition. This relation assumes that dendrite tip curvature effects and solid state diffusion are each negligible, thermodynamic equilibrium is maintained at the solid/liquid interface, and diffusion is infinitely fast in the liquid. The expression has been shown to provide a reasonably accurate description of microsegregation patterns in fully austenitic welds [5, 10, 11] where cooling rates are relatively high and diffusion is relatively slow. The value of k provides a measure of an element's microsegregation potential, where elements with lower k values segregate strongly to the

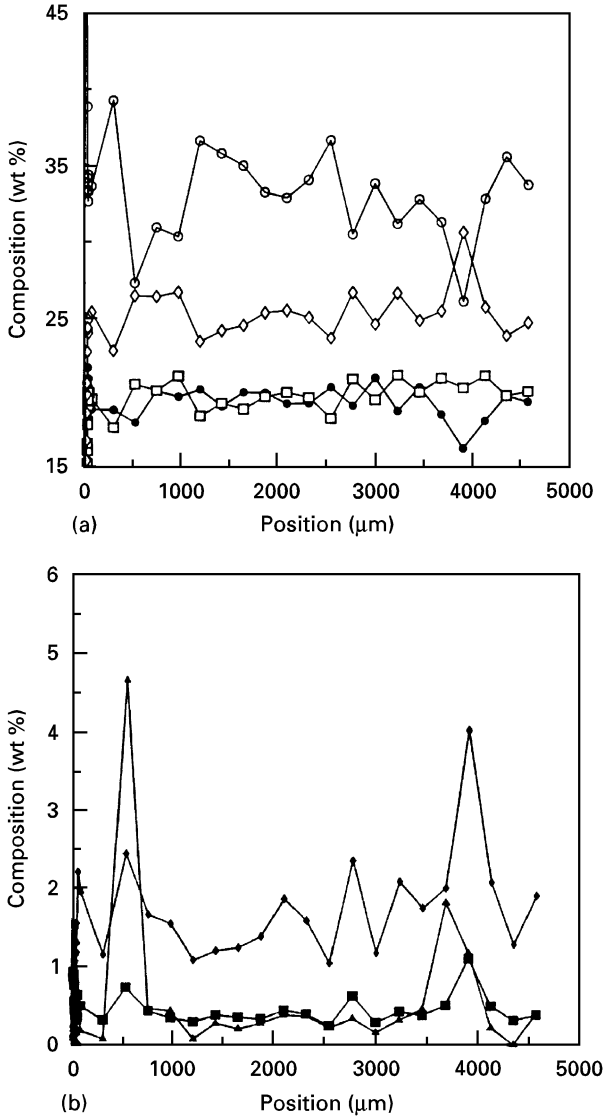

Figure 8 EPMA results from a trace conducted across the entire weld overlay. (a) Fe(○), Ni(◇), Co(●), and Cr(□); (b) Si(◆), Mo(■), and Ti(▲).

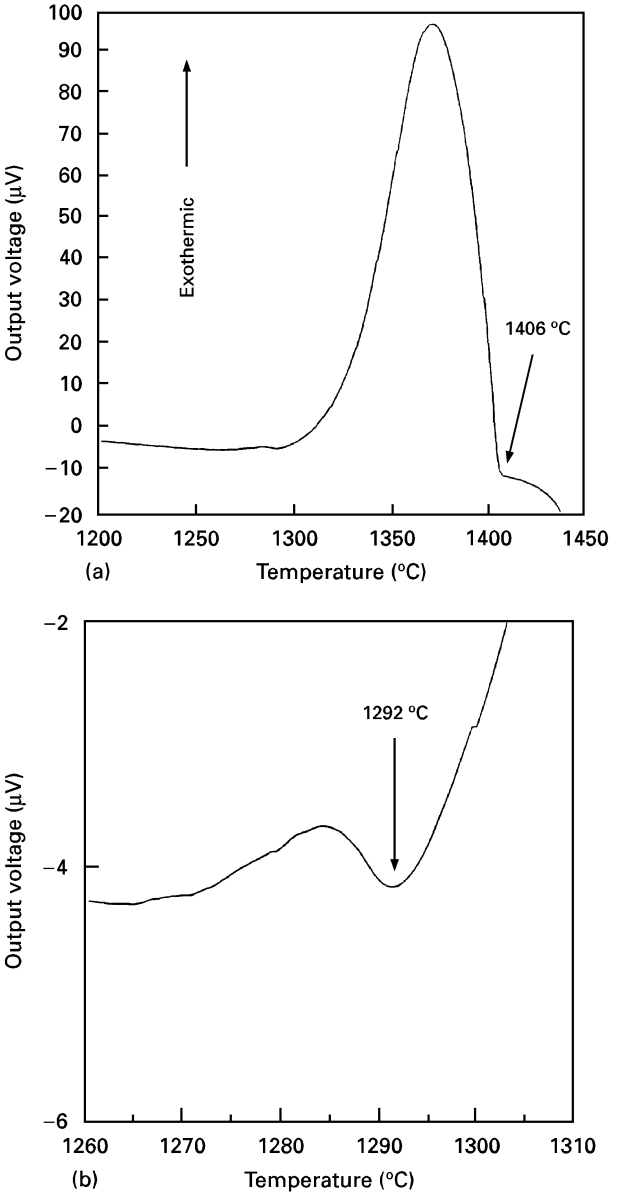

Figure 9 DTA solidification trace. (a) Overall view of solidification temperature range and (b) expanded view in the region of 1260 to 1310 °C.

TABLE II Results of wet chemical analysis and average values of EPMA data from weld overlay

Element	Chemical analysis	EPMA
Iron	32.91	32.9 ± 6.7
Nickel	25.83	25.3 ± 2.5
Chromium	19.22	19.9 ± 0.7
Cobalt	20.01	19.3 ± 1.1
Molybdenum	0.39	0.4 ± 0.1
Silicon	1.93	1.9 ± 0.9
Titanium	0.34	0.4 ± 0.2
Carbon	0.086	–
Sulfur	0.007	–
Phosphorus	0.008	–

All values in wt %.

TABLE III Initial distribution coefficients, k, of several elements in HR-160 weld overlay compared with Incoloy 909

Element	HR-160 weld overlay (this work)			Incoloy 909 [11]	
	C_0	C_s @ $f_s = 0$	k	C_0	k
Iron	32.91	37.53	1.14	40.89	1.10
Nickel	25.83	23.79	0.89	38.83	0.97
Chromium	19.22	19.02	0.99	–	–
Cobalt	20.01	21.54	1.08	12.61	1.02
Molybdenum	0.39	0.28	0.72	–	–
Silicon	1.93	1.02	0.53	0.48	0.67
Titanium	0.34	–	–	1.50	0.65

All values in wt %.

liquid phase during solidification and induce steeper concentration gradients in the final weld metal microstructure.

Values of k at the initiation of solidification can be determined by noting that, in Equation 1, $C_i = k_i C_o$ at $f_s = 0$, where C_i is the dendrite core composition (the first solid to form when $f_s = 0$) , k_i is the distribution coefficient at the start of solidification, and C_o is the nominal composition. C_i is measured by EPMA at the dendrite cores where the concentration is at

a minimum (for $k < 1$) and, as demonstrated above, the results from chemical analysis of the all weld metal deposit can be used as C_o because the overlay composition is uniform on a macroscopic scale (Fig. 8). These values are summarized in Table III. Comparison is made with the results previously reported by Cieslak *et al.* on Incoloy 909, a Co-containing Ni-based alloy [11]. The data show that the microsegregation potentials of elements in the two alloy systems are qualitatively similar, where Fe and Co each segregate to the solid during solidification ($k > 1$) and the remainder of the elements segregate preferentially to the liquid ($k < 1$). (A k value for Ti was not calculated here since the minimum concentration at the dendrite cores was below the EPMA detectability limit). The difference of primary importance lies within the lower value of k for Si determined for the HR-160 weld overlay.

The rather low value of k for Si should be considered with regards to possible influences on corrosion resistance. Silicon is added to promote the formation of a protective oxide surface scale in low P_{O_2} environments. Although the bulk HR-160 filler alloy contains 2.68 wt % Si (Table I), the final overlay deposit exhibits localized Si concentrations as low as $\approx$1 wt % (Fig. 5) due to combined effects of dilution and microsegregation. The effect of dilution is to reduce C_o in Equation 1 while microsegregation acts to produce locally depleted regions at the dendrite core due to the low k value in Equation 1. Since C_i, the dendrite core composition, is given by $C_i = kC_o$, low Si concentrations are produced at the dendrite cores by these combined factors. The bulk overlay composition, C_o can be maximized by minimizing dilution via control in processing parameters [13]. However, assuming k_{Si} does not vary significantly within the range of nominal Si concentrations of interest in weld overlay applications, the dendrite core compositions will always be about half of the bulk overlay composition in the as-solidified microstructure since $k_{Si} \approx 0.5$

5. Summary

The solidification behaviour of an HR-160 weld overlay deposited on 2.25Cr–1Mo steel has been examined. The weld overlay terminates solidification at $\approx$ 1290 °C by the formation of a (Ti, S)-rich second phase. The formation of solidification cracks in the overlay deposit are attributed to the extension of the solidification temperature range associated with the second phase and the semi-continuous distribution of the second phase along grain boundaries. The microsegregation behaviour of the main alloying elements in the overlay is similar to Incoloy 909, a Co-containing alloy of similar composition. In particular, the distribution coefficient for Si, an important alloying element for corrosion resistance, is $k_{Si} \approx 0.50$. This indicates that minimum Si concentration levels equal to about half the bulk overlay composition will exist in the dendrite cores of the as-solidified weld metal microstructure.

Acknowledgements

The author appreciates the financial support of this work by Pennsylvania Power & Light Co., Public Service Electric & Gas, Virginia Power, and Ohio Edison. Technical assistance of the EPMA work by Kathy Reppa and DTA work by Shaun Gauss of Lehigh University is also greatly appreciated.

References

1. G. Y. LAI, *J. Metals* **41** (1989) 21.
2. *Idem.*, "High temperature corrosion of engineering alloys" (ASM International, Materials Park, OH, 1990) p. 138.
3. S. C. KUNG, D. T. MARTIN, L. D. PAUL and K. K. HO, in Corrosion '92, NACE, Houston, TX, 1992. Paper No. 132.
4. J. C. BORLAND, *Brit. Welding J.* **7** (1960) 508.
5. J. A. BROOKS, in Proceedings of Weldability of Materials, October 8–12, 1990, ASM, p. 41.
6. Y. ARATA, F. MATSUDA and S. KATAYAMA, *Trans. Japan. Welding Res. Inst.* (1997) 105.
7. F. MATSUDA, H. NAKAGAWA, S. KATAYAMA and Y. ARATA, *Trans. Japan Welding Soc.* **13** (1982) 41.
8. M. J. CIESLAK and W. F. SAVAGE, *Welding J.* **64** (1985) 119s
9. D. A. CANONICO, W. F. SAVAGE, W. J. WERNER and G. M. GOODWIN, in "Effects of Minor Elements on the Weldability of High-Nickel Alloys" (Welding Research Council, New York, NY, 1969) p. 68.
10. G. A. KNOROVSKY, M. J. CIESLAK, T. J. HEADLEY, A. D. ROMIG, JR. and W. F. HAMMETTER, *Metall. Trans. A* **20A** (1989) 2149.
11. M. J. CIESLAK, T. J. HEADLEY, G. A. KNOROVSKY, A. D. ROMIG, JR. and T. KOLLIE, *ibid.* **21A** (1990) 479.
12. W. F. SAVAGE, E. F. NIPPES and G. M. GOODWIN, *Welding J.* **56** (1977) 245s
13. J. N. DUPONT and A. R. MARDER, *Metall. Trans. B*, **27B** (1996) 481.
14. E. SCHEIL, *Z. Metallk.* **34** (1942) 70.

Received 7 May
and accepted 19 December 1996